ACS OMEGA

http://pubs.acs.org/journal/acsodf

Article

Functionalized Electrospun Double-Layer Nanofibrous Scaffold for Wound Healing and Scar Inhibition

Changming Su,[§] Jing Chen,[*,§] Xianrui Xie, Zhongfei Gao, Zhenxin Guan, Xiumei Mo, Chunhua Wang,[*] and Guige Hou[*]

Cite This: *ACS Omega* 2022, 7, 30137−30148

Read Online

ACCESS | Metrics & More | Article Recommendations | Supporting Information

ABSTRACT: Considerable advances have been made in developing materials that promote wound healing and inhibit scar formation in clinical settings. However, some challenges, such as cumbersome treatment processes and determination of optimal treatment time, remain unresolved. Thus, developing a multifunctional wound dressing with both wound healing and scar inhibition properties is crucial. Here, we present an integrated electrospun fibrous composite membrane (MPC12) for wound healing and scar inhibition, consisting of a quaternized chitosan-loaded inner membrane (PCQC5) and quaternized silicone-loaded outer membrane (MQP12). The inner membrane effectively coagulates blood and promotes wound healing, and the outer membrane moisturizes, resists bacteria, and inhibits scar formation. *In vivo* evaluation in a rabbit ear model revealed that MPC12 treatment results in faster wound healing and better alleviation of scar hypertrophy than treatment with commercial products (KELO-COTE and MSSG). Our strategy offers an excellent solution for the potential integration of wound healing and scar inhibition.

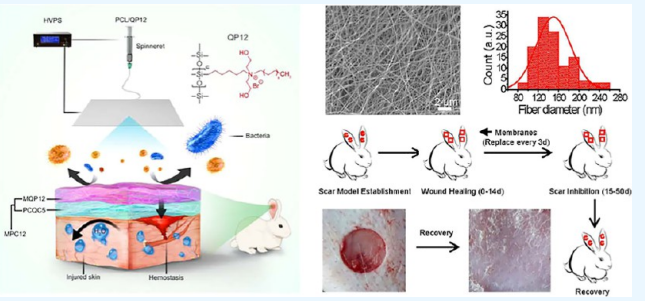

1. INTRODUCTION

The skin is the largest organ in the human body.[1] It is the first barrier against any damage from the environment.[2−4] According to the National Center for Health Statistics, human skin wounds have become a major threat to public health and the economy.[5] Wound healing is a complex process affected by internal and external factors, and an appropriate environment is needed to achieve accelerated healing.[6] However, tissue scarring, connective tissue response to surgery, trauma, inflammation, or burn injuries are intractable challenges for dermatologists and plastic surgeons.[7−9] Moreover, patients with excessive cell proliferation, abnormal cell growth, and aberrant deposition of collagen generally experience physical and psychosocial consequences.[10]

Advances in medical technology have enabled the development of several effective materials for wound dressing to achieve rapid wound closure; these include materials of animal or herbal origin and synthetic dressings.[11−13] These wound dressings control bleeding quickly but lead to excessive collagen deposition during wound healing. Thus, they neither maintain the balance between collagen secretion and degradation nor provide the necessary moist environment to help scar inhibition.[14] Current approaches for preventing scars generally include scar dressing after wound healing because its use before wound healing is highly inflammatory. Additionally, the best time to use scar dressing after wound healing is difficult to determine, which limits its clinical applications. Wound dressing technology is not commensurate with the current level of medical care provided. Thus, there is a need for a multifunctional wound dressing with wound and scar repair functions.

Materials with properties, such as skin adhesion, limited water vapor penetration, stratum corneum hydration, and oxygen penetration, help inhibit scar formation.[9,15−18] Polydimethylsiloxane (PDMS), the main component in silicone, has been accepted as a biomaterial for scar suppression owing to its excellent hydrophobicity, non-toxicity, and non-irritant behavior.[19,20] However, its strong inflammatory properties restrict its widespread application to newly formed wounds, as the suitable time for its application to facilitate scar repair can be easily misinterpreted. Moreover, PDMS cannot effectively resist bacterial invasion and is prone to wound infection. The structure of PDMS is stable and difficult to modify. Therefore, improving the antibacterial properties of PDMS and reducing the associated skin irritation have become important issues.

Received: May 24, 2022
Accepted: August 5, 2022
Published: August 18, 2022

https://doi.org/10.1021/acsomega.2c03222
ACS Omega 2022, 7, 30137−30148

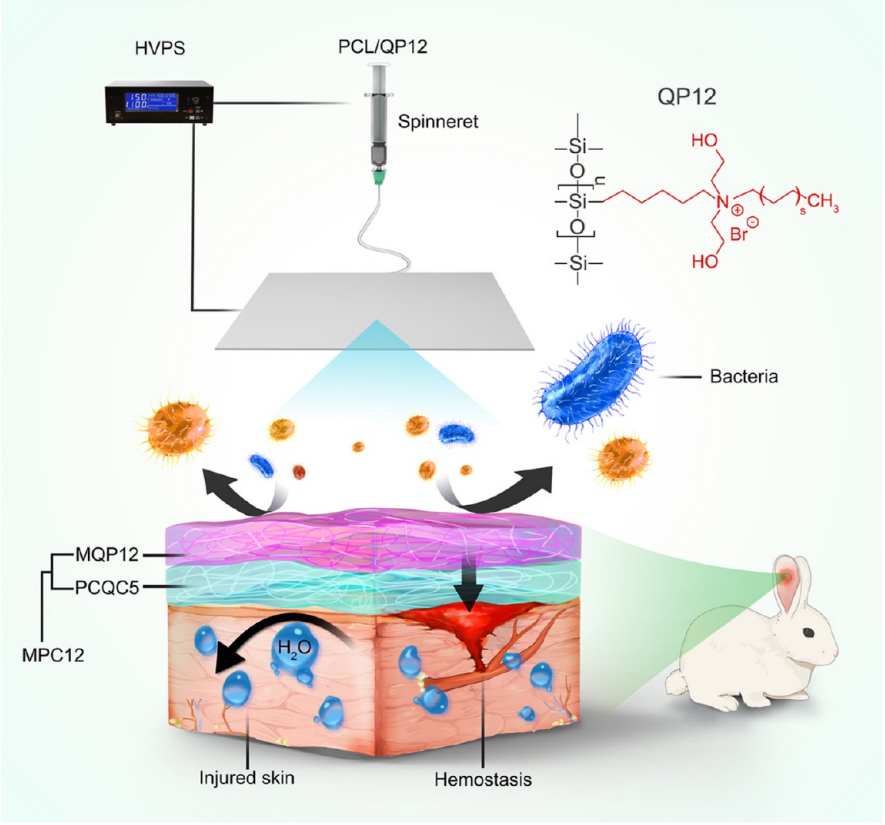

Figure 1. Schematic illustration of MPC12 nanofiber composite membrane design. The design for the integration of wound healing and scar inhibition in a rabbit ear wound model.

Quaternary ammonium salts (QAS) possess biocidal activities and have been widely used for more than half a century to control microbial growth.[21,22] The mechanism involves electrostatic and lipophilic interactions with the cell wall of various microorganisms. In addition, the chemical structure of QAS plays an important role in antibacterial activity because the effect of QAS with long hydrophobic chains on the outer membrane of Gram-negative bacteria is more profound than that of short-chain analogues.[23,24] Previous investigations have demonstrated that surfaces coated with a polymer containing QAS kill a variety of microorganisms, including Gram-positive bacteria, Gram-negative bacteria, yeasts, and molds.[25−27]

Considering that polymethyl hydrogen siloxane (PMHS) has a structure similar to that of PDMS with good water retention and is gas permeable and chemically inert, it has been widely used as a scar suppression material. The electrospinning technique is a fabrication method widely used to generate tissue-engineering scaffolds owing to their nanoscale morphology, high porosity, and large specific surface area.[28−30] We synthesized quaternized silicone (QP12) based on PMHS by introducing QAS into the polymer side chain to resist bacterial invasion. The outer layer [poly(ε-caprolactone) [PCL]/QP12, MQP12] of the composite membrane with antibacterial invasion and water-retaining functions, based on QP12 and PCL, was prepared *via* electrospinning (ES). Chitosan (CS) has been widely used as a functional biopolymer in biological scaffolds, pharmaceutical engineering, bone healing materials, and wound dressings owing to its excellent biocompatibility, antibacterial activity, and biodegradability. Recently, we prepared a wound repair membrane PVC/COL/QAS-CS (PCQC5) based on polyvinyl alcohol (PVC), collagen (COL), and quaternized chitosan (QAS-CS) with rapid hemostatic and anti-inflammatory functions.[28] Hence, we performed ES with MQP12 and PCQC5 to produce a double-layer nanofiber dressing (MPC12) for integrated wound repair and scar suppression. We aimed to successfully produce and test MPC12 for cytocompatibility and skin irritant properties using both *in vitro* and *in vivo* therapeutic evaluations to simultaneously achieve wound healing and scar suppression with a higher therapeutic index and fewer adverse effects (Figure 1).

2. MATERIALS AND METHODS

2.1. Materials. Chitosan, PMHS, diethanolamine, chlorhexidine acetate (CA), and benzalkonium chloride (BZK) were purchased from Shanghai Macklin Biochemical. 1-Bromododecane and hexafluoroisopropanol were obtained from Shanghai Aladdin Biochemical. 6-Bromo-1-hexene and PCL were obtained from Sigma-Aldrich. Yeast powder, tryptone, and Sabouraud agar medium were obtained from the British OXOID company. Fetal bovine serum and 3-(4,5-dimethylthiazol-2-yl)-2,5-diphenyltetrazolium bromide (MTT) were procured from Gibco. Dulbecco's modified Eagle medium (DMEM), Roswell Park Memorial Institute 1640 (RPMI 1640), and trypsin were purchased from the American Hyclone Company. All reagents were used without further purification unless otherwise specified.

2.2. Preparation and Characterization of MQP12 and MPC12 Membranes. PCL and QP12 were mixed with hexafluoroisopropanol at different proportions (PCL/QP12 = 100:0, 80:20, 75:25, 70:30, 60:40, 55:45, 50:50, and 40:60) to

https://doi.org/10.1021/acsomega.2c03222
ACS Omega 2022, 7, 30137−30148

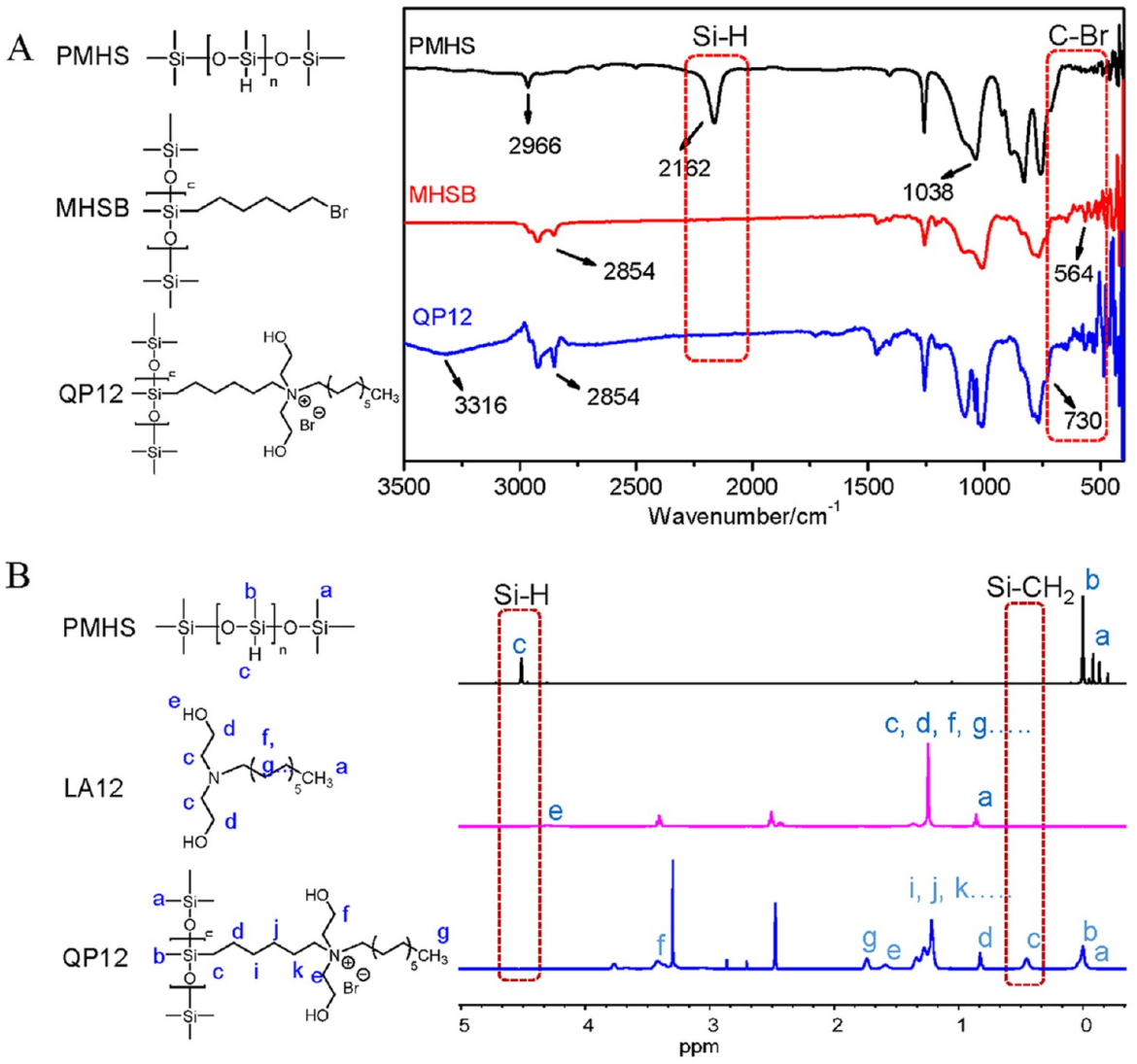

C

Compounds	*S. aureus*		*α-H. tococcus*		*E. coli*		*P. aeruginosa*		*P. vulgaris*		*C.albicans*	
	MIC	MBC	MIC	MBC	MIC	MBC	MIC	MBC	MIC	MBC	MIC	MBC
QP12	50	100	200	200	200	400	200	400	200	400	100	200
MHSB	>800	>800	>800	>800	>800	>800	>800	>800	>800	>800	>800	>800
BZK	3.125	6.25	6.25	12.5	25	50	12.5	50	25	50	25	25
CA	3.125	3.125	3.125	6.25	25	50	25	50	25	50	12.5	25

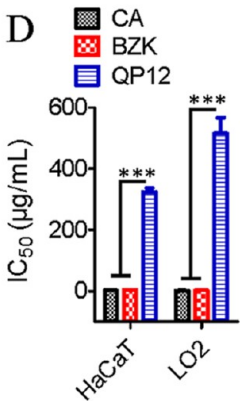

Figure 2. Characterization of QP12. (A) FT-IR spectra of PMHS, MHSB, and QP12. (B) ^{1}H NMR spectra of PMHS, LA12, and QP12. (C) MIC (μg/mL) and MBC (μg/mL) of CA, BZK, and QP12 in *S. aureus*, α-H. Tococcus, *E. coli*, *P. aeruginosa*, *P. vulgaris*, and *C. albicans*. (D) Cytotoxicity of QP12 toward HaCaT and LO2 cell lines after 24 h of culture. Data are presented as the mean ± SD, ***$p < 0.001$ (*t*-test). FT-IR, Fourier transform infrared; PMHS, polymethyl hydrogen siloxane; MHSB, PMHS grafted with bromohexane; QP12, quaternized silicone; ^{1}H NMR, proton nuclear magnetic resonance; LA12, *N*,*N*-dihydroxyethyl-*N*-dodecyl-tertiary amine; MIC, minimum inhibitory concentration; MBC, minimum bactericidal concentration; CA, chlorhexidine acetate; BZK, benzalkonium chloride; HaCaT, human immortalized epidermal cells; LO2, normal human liver cells; SD, standard deviation.

yield a 6 wt % solution or mixed at an indicated ratio (PCL/QP12 = 70:30) to yield solutions of different concentrations (4, 5, 6, and 7 wt %). During the ES process, the precursor solution was pulled into a spinneret using a nozzle with a diameter of 0.6 mm. The spinneret was fixed to a precision pump and connected to the positive electrode of the high-

https://doi.org/10.1021/acsomega.2c03222
ACS Omega 2022, 7, 30137−30148

voltage power supply to maintain a steady flow rate of 1.0 mL/h. The ES voltage applied between the spinneret and the collector was 15 kV, and the distance was 13 cm. The prepared MQP12 nanomembrane was stored in a vacuum drying cabinet and dried at 25 °C for 3 days to remove residual solvent. MPC12 nanofiber composite membrane was obtained by spinning MQP12 onto PCQC5 membrane under the same conditions. The morphology and diameter of the MQP12 and MPC12 membranes were characterized using SEM and AFM. The existence of PCL and QP12 in MQP12 was determined *via* DSC and FT-IR spectroscopy. The thermal stability of MQP12 was characterized using TGA. Mechanical properties of MPC12 were evaluated using a tensile mechanical analyzer at a fixed speed of 10 mm min^{-1} at 25 °C and 50% relative humidity. The surface wettability of the inner and outer layers of the MPC12 membranes was evaluated using the WCA analysis. Water droplets of diameter 6 μm were separately dripped onto the surface of the nanofibrous membranes at 25 °C and measured within 5 s.

2.3. Microbial Invasion on the Membrane. The nanomembrane was cut into small square pieces (1 cm × 1 cm) and placed in a solid medium after sterilization in such a way that one side was close to the culture medium. Representative strains of Gram-positive bacteria (*Staphylococcus aureus*), Gram-negative bacteria (*Escherichia coli*), and fungi (*Candida albicans*) were selected. Microbial solution (100 μL) at a concentration of 1.5×10^8 CFU mL^{-1} was inoculated on the outer side of the nanomembrane and incubated in an inverted culture for 8, 12, and 24 h. For SEM, the nanomembranes were uncovered and fixed with 2.5% glutaraldehyde for more than 4 h at 4 °C. After washing three times with PBS, the nanomembranes were dehydrated through sequential treatments with 50, 75, 85, 95, and 100% ethanol. The final samples were dried in a vacuum freezing/drying oven before SEM analysis.

2.4. Wound Healing and Scar Inhibition *In Vivo*. *In vivo* experiments were conducted by following guidelines approved by the ethics committee of Yantai Raphael Biotechnology Co., Ltd. (SYXK(Lu) 2017 0026). Female rabbits were used in this experiment. Three circular wounds with a full-thickness skin defect were created on the ventral surface of each ear and kept under sterile conditions. After thoroughly disinfecting the wounds, the animals were randomly divided into six groups. The negative control group was treated surgically, and then, medical gauze was applied. The positive control drugs (KELO-COTE and MSSG) were evenly applied to the wounds. The experimental drugs (MQP12, PCQC5, and MPC12) were applied as 2.0 × 2.0 cm square membranes to the wound surface, and medical bandages were used for fixation. The drugs in all groups were changed every 24 h. Digital camera images and rulers were used to record wound healing and scar suppression.

2.5. Statistical Analysis. All experimental data are presented as the mean ± standard deviation (SD), and the statistical significance between different groups was analyzed using a two-tailed unpaired Student's *t*-test with values of $*p < 0.05$, $**p < 0.01$, and $***p < 0.001$.

3. RESULTS AND DISCUSSION

3.1. Synthesis and Characterization of QP12. To improve antibacterial properties and biocompatibility of the outer composite membrane, the structure of PMHS was first modified by introducing a quaternary ammonium salt into the side chain, which resulted in PMHS derivatives (QP12). As depicted in Scheme S1, QP12 was prepared by following a three-step procedure, where LA12 was first synthesized using diethanolamine and 1-bromododecane. Next, the PMHS side chain was extended through a hydrolyzation reaction to obtain MHSB. Subsequently, MHSB was successfully reacted with the self-made tertiary amine LA12 to prepare QP12 with the active group at the end of the side chain. We determined the structures of PMHS, MHSB, and QP12 *via* FT-IR spectroscopy based on the vibration of different chemical bonds (Figure 2A). The absorption peak of PMHS at 2162 cm^{-1} was assigned to the Si−H stretch. This peak disappeared in MHSB and QP12, indicating that 1-bromododecane was successfully grafted onto PMHS. Compared with MHSB, the intensity of the C−Br peak near 560 cm^{-1} in QP12 was substantially reduced, and the characteristic peak of the long-chain alkyl group appeared at 730 cm^{-1}, which proved that QP12 was successfully formed *via* the reaction of LA12 with MHSB. The structures of PMHS, LA12, and QP12 were further determined by ^{1}H NMR according to different chemical environments, in which the H atom was located. It is evident from Figure 2B that the Si−H chemical shift at 4.5 ppm in PMHS disappeared in QP12 and the hydrogen on Si−CH_2− at 0.5 ppm appeared, confirming the successful hydrolyzation reaction. In addition, the presence of hydrogen with a chemical shift similar to that of LA12 in QP12, such as the hydrogen of −CH_2− in the dodecyl chain at 1.3 ppm, proved that PMHS was successfully quaternized. The grafting rate of QP12 was obtained using the elemental analysis, and the results showed that LA12, containing N, was successfully grafted to MHSB at a grafting rate of 15−23% (Table S1).

As the main component of the outer layer of the composite membrane, the minimum inhibitory concentration (MIC) and minimum bactericidal concentration (MBC) of QP12 were determined. Gram-positive bacteria (*S. aureus* and α-hemolytic *Streptococcus*), Gram-negative bacteria (*E. coli*, *Pseudomonas aeruginosa*, and *Proteus vulgaris*), and a fungus (*C. albicans*) were used to evaluate the antibacterial and antifungal activities. As shown in Figure 2C, the antibacterial performance of QP12 significantly improved compared with that of MHSB without quaternization. Two drugs, chlorhexidine acetate (CA) and benzalkonium chloride (BZK), were also used as positive controls. Although QP12 showed weaker antibacterial activity than CA and BZK, it showed enhanced antibacterial activity against the Gram-positive bacterium *S. aureus* and fungus *C. albicans* compared with that against other bacteria with MBC values of 100 and 200 μg mL^{-1}, respectively, and MIC values of 50 and 100 μg mL^{-1}, respectively.

QP12 was intended to be used as one of the main raw materials for the composite membrane in this study. Therefore, HaCaT and LO2 cell lines were selected to evaluate the epidermal and liver cytotoxicity of QP12 (Figure 2D). The IC_{50} values of QP12 in both cell lines were increased by 100-fold or more compared with those of the two positive controls. This indicated that QP12 was safer for normal mammalian cells than CA and BZK.

3.2. Preparation and Characterization of MQP12. ES technology has attracted considerable attention as an effective method to fabricate continuous and uniform nanofibers for wound dressing due to its merits, such as high surface-area-to-volume ratio, flexibility, and high attachment rate.[14,31,32] To obtain a better double-layer composite MPC12, we first optimized the conditions to prepare the outer membrane

https://doi.org/10.1021/acsomega.2c03222
ACS Omega 2022, 7, 30137−30148

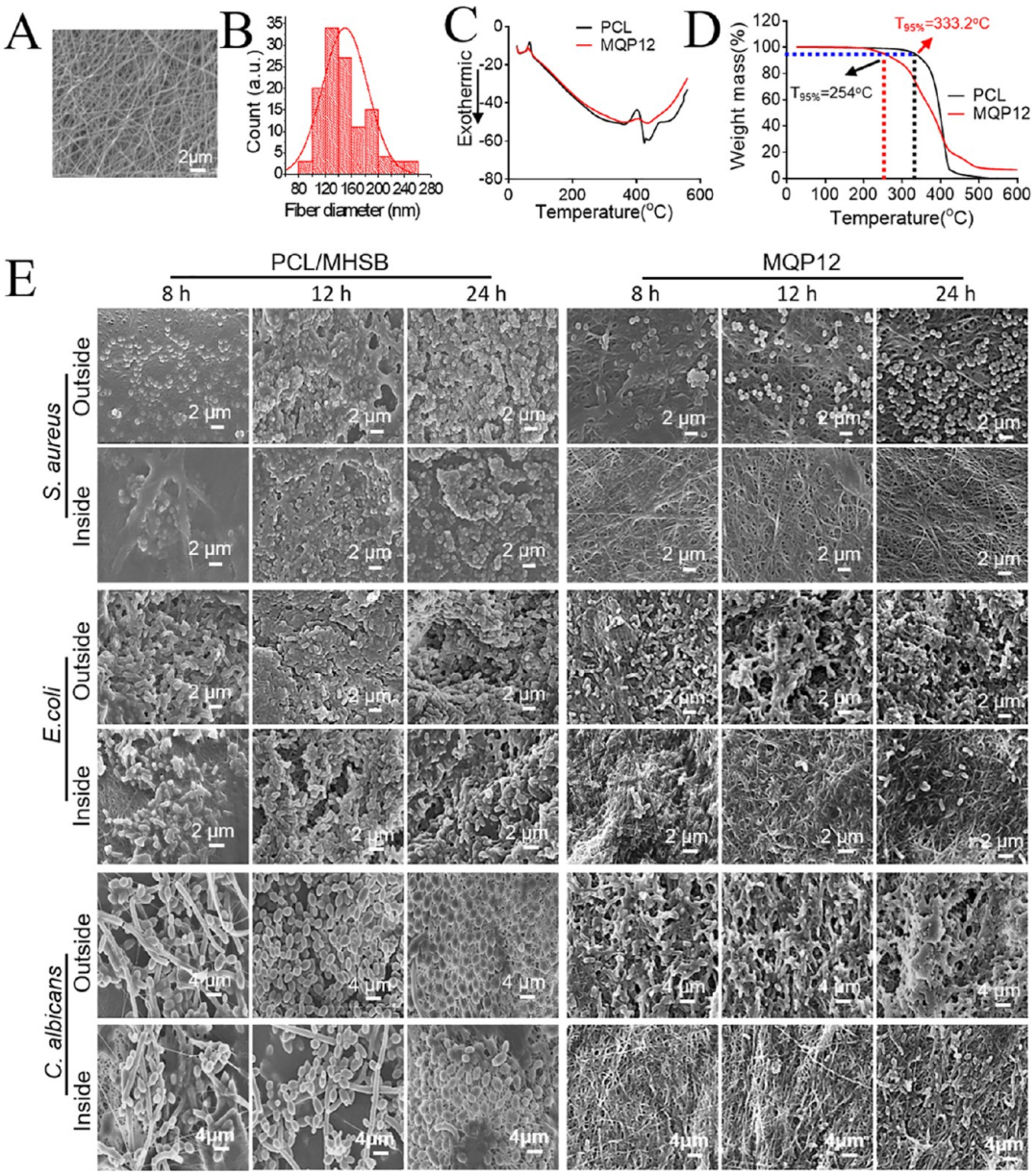

Figure 3. Synthesis and characterization of the MQP12 nanofiber membrane. (A) SEM image of the MQP12 membrane. (B) Fiber diameter distribution of MQP12. (C) DSC curves of PCL and MQP12 membranes. (D) TGA curves of PCL and MQP12. (E) SEM images showing the penetration ability of PCL/MHSB and MQP12 in *S. aureus*, *E. coli*, and *C. albicans* after culturing for 8, 12, and 24 h. SEM, scanning electron microscopy; MQP12, integrated electrospun fibrous composite membrane; DSC, differential scanning calorimetry; TGA, thermogravimetric analysis; PCL, poly(*ε*-caprolactone); MHSB, PMHS grafted with bromohexane.

MQP12. Due to the poor ES of the QP12 solution, PCL, which is approved by the US Food and Drug Administration as an ES fiber scaffold, was added to the solutions to assist MQP12 nanofiber formation. It is known that the polymer solution properties considerably influence the morphology and diameter of the nanofibers.[33−35] Adjusting the properties of the spinning solution to an appropriate range is important to obtain uniform electrospun nanofibers. Thus, we first focused on the ratios and concentrations of the ingredients in the spinning solution. The scanning electron microscopy (SEM) results shown in Figures 3A and S2 revealed that the best mass ratio of PCL/QP12 was 70:30, and the best concentration of the spinning solution was 7% (w/v). The viscosity of the spinning solution was evaluated using a viscometer with an average viscosity of 74 cP. The surface tension of the spinning solution was evaluated using a surface tension measuring device, and the surface tension value was 22.012 mN/m. The electric conductivity of the spinning solution measured using a conductivity meter was 75.1 μS/cm at 24.4 °C. Moreover, the uniform nanofiber membrane prepared under these conditions was reproducible with an average fiber diameter of 149.0 ± 3.33 nm (Figures 3B and S3).

To explore PCL/QP12 co-existence in the nanofiber membrane MQP12 and evaluate the specific heat capacity and transition heat, differential scanning calorimetry (DSC) was performed. We noticed that the melting point of PCL was approximately 62 °C, and the thermal decomposition temperature was 405.7 °C. After the addition of QP12, there was no distinct change in the characteristic peaks (Figure 3C), indicating that the incorporation of QP12 did not significantly

https://doi.org/10.1021/acsomega.2c03222
ACS Omega 2022, 7, 30137−30148

change the structure of PCL. We further characterized the functional groups in PCL, QP12, and MQP12 by FT-IR spectroscopy. As shown in Figure S4, almost all characteristic peaks in the infrared spectra of PCL and QP12 corresponded to the infrared spectra of MQP12, and no new characteristic peaks appeared for MQP12. These results proved that PCL and QP12 in the MQP12 fibers did not form a new chemical bond but existed in the fibers as a mixture. We next investigated the thermostability of MQP12 via thermogravimetric analysis (TGA). The decomposition temperatures (T_d) of PCL and MQP12 with 5% weight loss were 333.2 and 254.0 °C, respectively (Figure 3D). Thus, the electrospun nanofiber membranes of PCL and MQP12 were sufficiently stable to be used for high-temperature sterilization (usually <120 °C) and adhesion to human skin (usually ~37 °C).

For the outer layer of the composite membrane, the resistance of the nanofiber membrane to the microbial invasion was determined by comparing the permeation ability of the MQP12 membranes in *S. aureus*, *E. coli*, and *C. albicans* to that of the PCL/MHSB membranes. As the SEM images (Figure 3E) indicate, only a small number of microorganisms were found on the inner surface of MQP12 after culturing for 24 h, although this number was substantially increased on the outer surface. In contrast, all three microbial species had penetrated the PCL/MHSB nanomembrane inner surface after 8 h of culture, and as the culture time was prolonged, the microorganisms on the inner side of the PCL/MHSB membrane proliferated to form a biofilm. Notably, the inner surface of the MQP12 membrane was still sterile after 24 h of incubation with *S. aureus*, suggesting that the MQP12 membrane prevented *S. aureus* invasion, which was consistent with the antibacterial effect of QP12 on *S. aureus* in Figure 2C,D.

3.3. Preparation and Characterization of MPC12. The excellent complementary properties of MQP12 and PCQC5 encouraged us to combine them as a composite membrane that integrates wound healing and scar suppression. Therefore, we added MQP12 to the outer surface of our previously prepared PCQC5 to obtain MPC12 using ES according to the optimized conditions.[28] SEM images showed that both inner and outer layers of MPC12 were fibrous and had a uniform diameter; atomic force microscopy (AFM) images showed that R_a values of the outer and inner membranes of MPC12 were 72.8 and 95.1 nm, respectively, which had a certain degree of roughness suitable for cell adhesion (Figure 4A).

As mechanical properties have attracted attention because of their capability to modulate biological processes and determine cell fate,[36] we evaluated the mechanical properties of the MPC12 composite membranes. Three parts of the MPC12 nanofiber composite membrane were randomly selected. As shown in Figure 4B,C, the average tensile strength and strains at break of the MPC12 nanofiber composite films were 4.67 ± 1.06 MPa and 45.83 ± 2.96%, respectively. Ideal mechanical property and stretchability are essential in nanofiber wound dressings. The tensile strength and elasticity of the wound dressing should be similar to that of human skin to ensure close and comfortable contact with the wound and to regulate pulling forces applied to wounds. Normal human skin has tensile strengths ranging from 2 to 16 MPa and breaking strains of approximately 35−115%.[3,37] The MPC-12 nanofiber films are largely stretchable and therefore allow intimate contact with the wound surface.

The surface properties of the inner membrane and the outer membrane are among the main contributing factors in

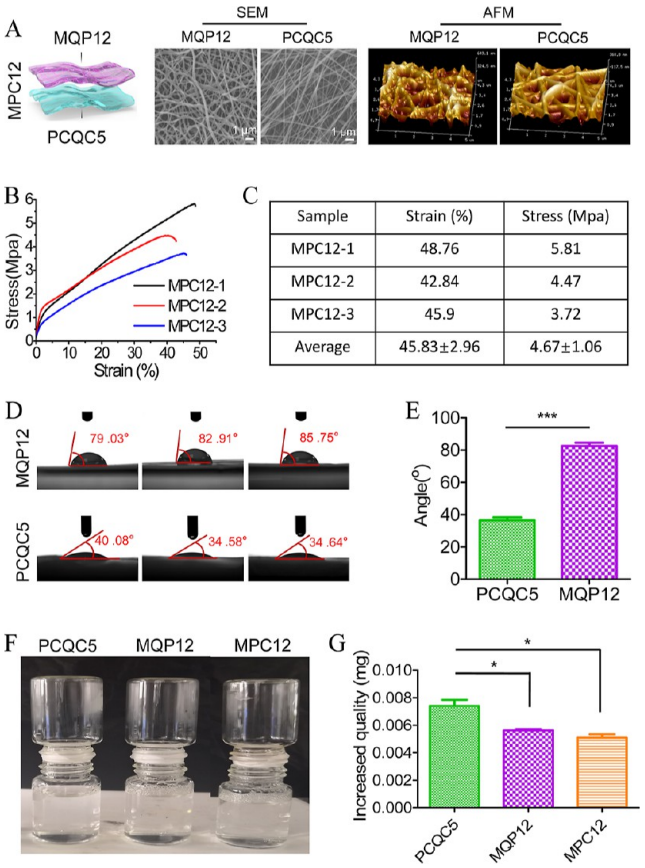

Figure 4. Synthesis and characterization of the MPC12 nanofiber composite membrane. (A) SEM and AFM images of the inner and outer layers of the MPC12 composite membrane. (B) Strain *vs* stress of MPC12 membranes was evaluated three times. (C) Average value of the strain and stress of the MPC12 membrane. (D) WCA analysis of MQP12 and PCQC5 nanofiber membranes. (E) Differences in the WCA analysis of MQP12 and PCQC5 nanofiber membranes. (F) Analysis of the water permeability of different membranes. (G) Quantification of the water passing through different membranes. Data are presented as the mean ± SD, ***$p < 0.001$ (*t*-test). SEM, scanning electron microscopy; AFM, atomic force microscopy; MPC12, electrospun fibrous composite membrane; MQP12, integrated electrospun fibrous composite membrane; WCA, water contact angle; SD, standard deviation.

integrated wound healing and scar suppression.[38] Therefore, we characterized the wettability of the inner membrane and the hydrophobicity of the outer membrane using water contact angle (WCA) analysis (Figure 4D,E). The results showed significant differences in the WCA of the two layers of the MPC12 nanofiber composite film. The average WCA of the inner layer was 82.56 ± 3.37°, whereas that of the outer layer was 36.43 ± 3.16°. Thus, the inner layer of MPC12 had excellent surface wettability, whereas the outer layer had a certain degree of hydrophobicity. A self-designed water permeation experiment and the corresponding quantitative results of water permeation also revealed similar results (Figure 4F,G). The inner membrane of MPC12 had superior permeability, which could promote cell adhesion and proliferation, as well as wound repair. The outer membrane displayed a water retention effect to prevent water volatilization, which can avoid excessive loss of skin moisture during wound repair to inhibit excessive fibroblast proliferation and collagen secretion.

https://doi.org/10.1021/acsomega.2c03222
ACS Omega 2022, 7, 30137−30148

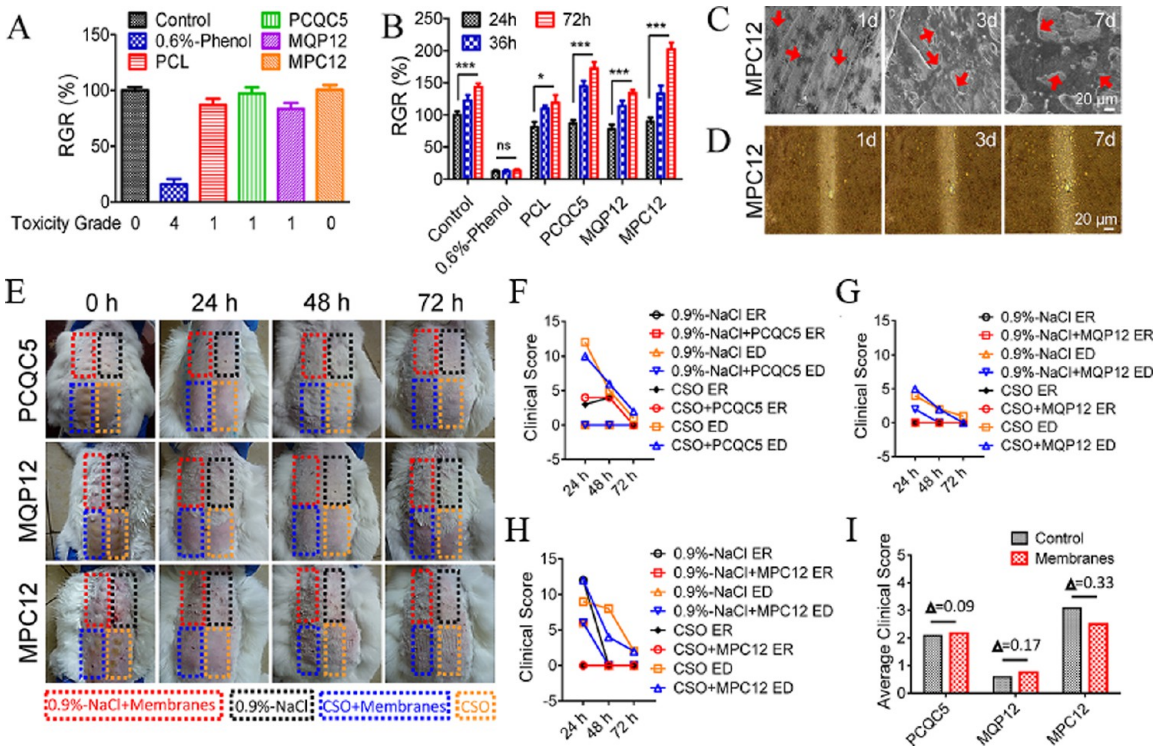

Figure 5. Biosafety evaluation of the nanofiber composite membrane. (A) Toxicity of different membranes to HaCaT cells after 24 h of incubation. (B) Relative growth rate of HaCaT cells after culturing with different membrane extraction liquids for 24, 48, and 72 h. (C) SEM images of HaCaT cell proliferation and morphological analysis of MPC12 nanofiber membranes after 1, 3, and 7 days. Red arrows indicate the cell monolayer boundary. (D) Microscopic images of HaCaT cell migration on the MPC12 nanofiber membranes after 1, 3, and 7 days. (E) Images of dorsal skin in different treatment groups at 0, 24, 48, and 72 h. Clinical score *vs* time for each rabbit in groups treated with PCQC5 (F), MQP12 (G), and MPC12 (H). (I) Average clinical scores of the rabbits in each treatment group at the end of therapy. Data are presented as the mean ± SD, $*p < 0.05$, $***p < 0.001$ (*t*-test). HaCaT, human immortalized epidermal cells; SEM, scanning electron microscopy; MPC12, electrospun fibrous composite membrane; MQP12, integrated electrospun fibrous composite membrane.

We also evaluated blood coagulation on the nanofiber membranes by testing the blood-clotting index and hemostatic ability. Only PCQC5 and PCQC5-containing MPC12 showed a low blood-clotting index, indicating better clotting capacity (Figure S5). This was likely because our previously prepared wound healing dressing, PCQC5, had excellent coagulation properties. In addition, we established rabbit arterial auricular and liver hemorrhage models to investigate the hemostatic ability of MPC12. Compared with medical gauze and medical gelatin sponge, MPC12 effectively reduced bleeding (Figure S6).

3.4. Biosafety Evaluation of MPC12. Toxicity evaluation of MPC12 is critical for its further clinical application. We assessed cytotoxicity, blood compatibility, and skin irritation to evaluate any potential biohazards associated with the prepared composite membrane. According to the cytotoxicity evaluation grade (GB/T 16886.5) (Table S2), the cytotoxicity of different composite membranes on the immortalized epidermal cell HaCaT was graded (Figure 5A). The relative growth rate of HaCaT cells on the MPC12 nanofiber composite membrane extract was 100.5% similar to that of the control. MPC12 showed 0-grade cytotoxicity, indicating that it was suitable for biological applications.

Although the cells cultured in MPC12 extract proliferated slowly in the first 24 h, HaCaT cell proliferation increased significantly after 72 h of culture (Figure 5B). The HaCaT cells gradually spread on the surface of MPC12 over time and almost formed a cell monolayer after 7 days of culture (Figure 5C). This indicated that MPC12 with low cytotoxicity and strong cell adhesion might have potent efficacy in promoting cell proliferation. The cell migration on MPC12 was characterized (Figure 5D). The results showed that HaCaT cells could cross the scratches after 7 days of culture, indicating that the membrane is beneficial to cell migration.

To further ensure the feasibility of MPC12 *in vivo*, its blood compatibility was evaluated using H_2O as the positive control and 0.9% NaCl as the negative control (Figure S7). The hemolysis rate of the membranes in all experimental groups was lower than 5%, which met the standards of GB/T16886.4 for biomedical material.

Before testing the MPC12 composite membranes in the integration of wound repair and scar suppression, we also assessed skin irritation *in vivo*. For this purpose, the dorsal skin of four healthy rabbits was injected with 0.9% NaCl extract of different membranes and cottonseed oil (CSO) extract of different membranes, and 0.9% NaCl and CSO were used as controls. As shown in Figure 5E, skin redness and swelling were observed 24, 36, and 72 h after injection and were scored (Figure 5F–H) according to the degree of skin erythema and edema at each injection site (GB/T16886.10) (Table S3). As shown in Figure 5I, the difference in the comprehensive average scores of PCQC5, MQP12, and MPC12 at the three time points for the two solvent extracts and the control group was less than one. Thus, MPC12 did not cause any obvious skin irritation as a skin dressing. Overall, these results

https://doi.org/10.1021/acsomega.2c03222
ACS Omega 2022, 7, 30137−30148

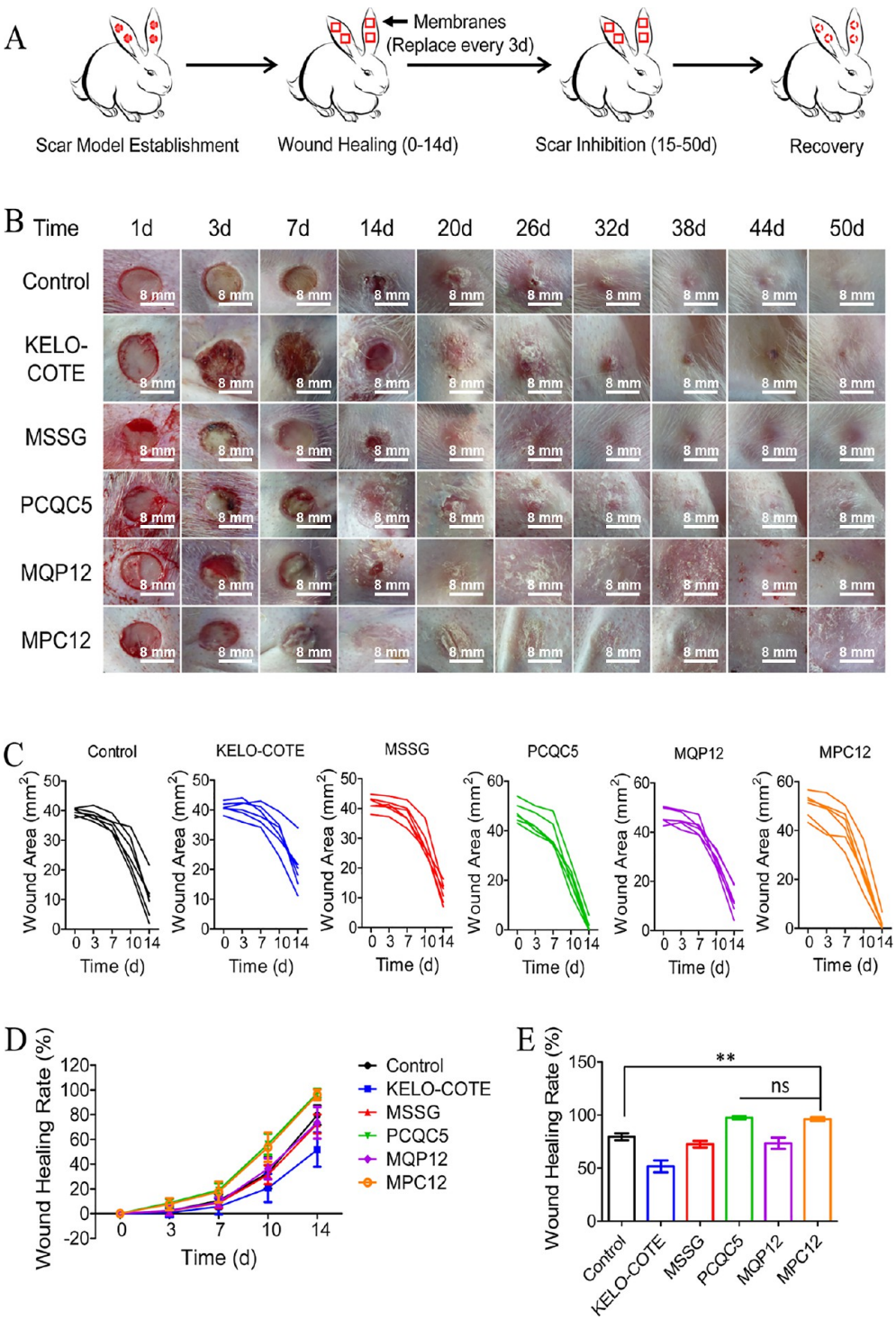

Figure 6. Wound healing and scar inhibition in the rabbit ear model. (A) Experimental outline of wound healing and scar inhibition. (B) Photographs of the wounds in different treatment groups at different time points. (C) Changes around each wound in the first 14 days of treatment in the control, KELO-COTE, MSSG, PCQC5, MQP12, and MPC12 groups. (D) Wound healing rates in each group. (E) Average wound healing rate in each treatment group at the end of therapy. Data are presented as the mean ± SD, $^{**}p < 0.01$ (*t*-test). MQP12, electrospun fibrous composite membrane; MQP12, integrated electrospun fibrous composite membrane; SD, standard deviation.

demonstrated that MPC12 had superior biosafety and caused extremely low skin irritation.

3.5. Wound Healing and Scar Inhibition *In Vivo*. Next, we evaluated the integrated efficiency of the MCP12 membranes in promoting wound healing and inhibiting wound scar formation in a rabbit ear model and compared it with that of related commercial products (KELO-COTE and MSSG) (Figure 6A).[38,39] Full-thickness skin wounds were created on each ear, and the rabbits were randomly divided into the following six groups: control, KELO-COTE, MSSG, PCQC5, MPQ12, and MPC12. The size of the wounds was recorded after the operation using a digital camera. As shown in Figure 6B, the wounds treated with PCQC5 and MPC12 were already covered by neotissue 14 days after the treatment,

https://doi.org/10.1021/acsomega.2c03222
ACS Omega 2022, 7, 30137−30148

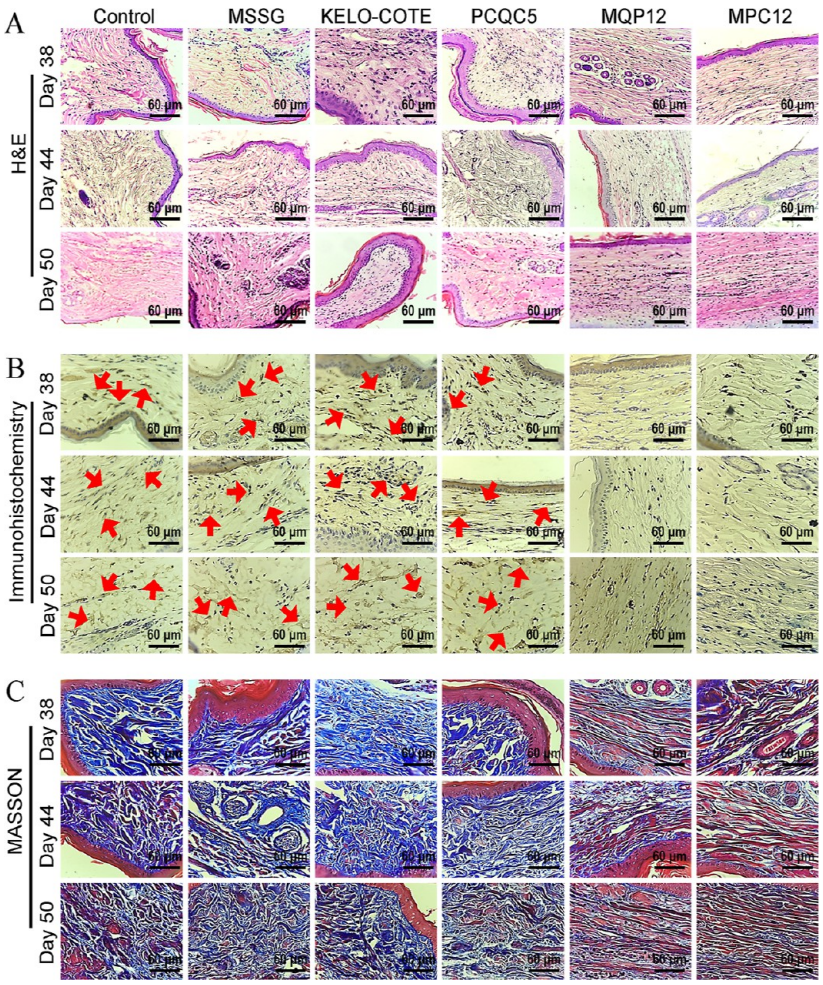

Figure 7. Histological appearance of newly formed skin tissues in each group at different time points. (A) H&E staining of tissue sections after 38, 44, and 50 days. (B) Immunohistochemical staining for TNF-α at 38, 44, and 50 days. Red arrows indicate positivity. (C) Masson staining of the newly formed skin around the wound after 38, 44, and 50 days. H&E, hematoxylin and eosin.

whereas the wounds in all other groups still had an obvious defect. The changes in the wound area during the treatment were also measured using calipers as an indicator of the wound healing progress (Figure 6C). Two weeks post operation, the wound healing rates of PCQC5 and MPC12 were 97.47% ± 3.56 and 96.20% ± 4.29%, respectively, whereas those of the control, KELO-COTE, MSSG, and MPQ12 groups were 79.58 ± 7.98, 51.74 ± 13.79, 72.52 ± 7.54, and 73.47 ± 12.90%, respectively (Figure 6D). Overall, the rabbits treated with PCQC5 and MPC12 exhibited significantly higher treatment efficiency at the end of the therapy (Figure 6E). In contrast, the rabbits treated with KELO-COTE, MSSG, and MPQ12 exhibited lower healing efficiency, indicating that scar-inhibiting membranes with moisturizing functions were not conducive to wound healing.

It is worth noting that the surface of the wounds treated with MPC12 was smooth and the entire amount of the newly formed skin did not significantly increase after approximately 7 weeks of continuous treatment. Thus, we further evaluated the state of scar formation *via* hematoxylin and eosin (H&E) staining using samples resected at 38, 44, and 50 days, as the histopathological analysis provides a microscopic view of the scar formation process.[40] The microscopic evaluation indicated that the wound sites showed different tissue arrangements after treatment with different dressings. As shown in Figure 7A, the internal fibers in the groups treated with MQP12 and MPC12 were arranged tightly and orderly, whereas the tissue fibers were disordered and accompanied by mild chronic inflammation in the groups with a scar where the tissue protruded from the skin surface. Thus, MPC12 promoted regularized tissue repair and avoided the formation of hyperplastic scars. As scar formation is always accompanied by inflammation, the expression of the inflammatory factor TNF-α in the wound tissues was detected *via* immunohistochemistry to indirectly reflect the state of scar suppression.[41−43] The expression of TNF-α was high in the control, KELO-COTE, MSSG, and PCQC5 groups, and it did not significantly decrease within 50 days, whereas the inflammatory response in the MQP12 and MPC12 groups was negligible (Figure 7B). We finally observed collagen deposition in the newly formed tissues *via* Masson staining, as abnormally excessive collagen deposition is an important feature of scar formation.[44,45] From 38 to 50 days post operation, the expression of collagen type I in the tissues of the MQP12 and MPC12 groups gradually decreased, with many muscle fibers appearing in the tissues. In contrast, all other groups showed excessive secretion of collagen type I with some muscle fiber production (Figure 7C). All histology results were consistent with the macroscopic evaluation in Figure 7A, indicating that the MPC12 membranes not only

https://doi.org/10.1021/acsomega.2c03222
ACS Omega 2022, 7, 30137−30148

promoted wound healing but also had excellent scar suppression ability.

4. CONCLUSIONS

Based on the integration of wound healing and scar repair, we successfully fabricated an MPC12 nanofiber composite membrane by adding MQP12 on the outer surface of our previously prepared PCQC5 using ES. Mechanical properties of the MPC12 composite membrane are similar to those of the skin, and the membrane offers suitable hydrophobicity/hydrophilicity for wound healing and scar repair. Antimicrobial invasion and hemostatic experiments proved that the outer membrane of the composite membrane effectively resists bacterial invasion, whereas the inner membrane has a rapid hemostasis function *in vitro*. Safety evaluation of MPC12 demonstrated superior biosafety and extremely low skin irritation, which is promising for its *in vivo* use. *In vivo* evaluation of wound healing and scar inhibition demonstrated that the MPC12 membrane can accelerate wound repair and inhibit scar formation. Our method is safer and more effective than traditional methods of treating hypertrophic scars, such as KELO-COTE and MSSG. We envision that MPC12 will provide an innovative approach for the integration of wound healing and scar inhibition and that it has a high potential for clinical translation.

■ ASSOCIATED CONTENT

Supporting Information

The Supporting Information is available free of charge at https://pubs.acs.org/doi/10.1021/acsomega.2c03222.

Preparation and characterization of nanofibrous scaffold; *in vitro* antibacterial; *in vitro* cytotoxicity and proliferation; *in vitro* blood coagulation; and *in vivo* animal experiments (PDF).

■ AUTHOR INFORMATION

Corresponding Authors

Jing Chen − *School of Pharmacy, Key Laboratory of Prescription Effect and Clinical Evaluation of State Administration of Traditional Chinese Medicine of China, Binzhou Medical University, Yantai 264003, People's Republic of China*; orcid.org/0000-0002-1432-8213; Email: chenjingbyyxy@163.com

Chunhua Wang − *School of Pharmacy, Key Laboratory of Prescription Effect and Clinical Evaluation of State Administration of Traditional Chinese Medicine of China, Binzhou Medical University, Yantai 264003, People's Republic of China*; Email: chunhuawang508@126.com

Guige Hou − *School of Pharmacy, Key Laboratory of Prescription Effect and Clinical Evaluation of State Administration of Traditional Chinese Medicine of China, Binzhou Medical University, Yantai 264003, People's Republic of China*; orcid.org/0000-0002-9493-3981; Email: guigehou@163.com

Authors

Changming Su − *School of Pharmacy, Key Laboratory of Prescription Effect and Clinical Evaluation of State Administration of Traditional Chinese Medicine of China, Binzhou Medical University, Yantai 264003, People's Republic of China*

Xianrui Xie − *School of Pharmacy, Key Laboratory of Prescription Effect and Clinical Evaluation of State Administration of Traditional Chinese Medicine of China, Binzhou Medical University, Yantai 264003, People's Republic of China*

Zhongfei Gao − *School of Pharmacy, Key Laboratory of Prescription Effect and Clinical Evaluation of State Administration of Traditional Chinese Medicine of China, Binzhou Medical University, Yantai 264003, People's Republic of China*

Zhenxin Guan − *School of Pharmacy, Key Laboratory of Prescription Effect and Clinical Evaluation of State Administration of Traditional Chinese Medicine of China, Binzhou Medical University, Yantai 264003, People's Republic of China*

Xiumei Mo − *State Key Laboratory for Modification of Chemical Fibers and Polymer Materials, College of Chemistry, Chemical Engineering and Biotechnology, Donghua University, Shanghai 201620, People's Republic of China*; orcid.org/0000-0001-9238-6171

Complete contact information is available at: https://pubs.acs.org/10.1021/acsomega.2c03222

Author Contributions

[§]C.S. and J.C. contributed equally to this work.

Notes

The authors declare no competing financial interest.

■ ACKNOWLEDGMENTS

This work was supported by the Key R&D Program of Shandong province [grant number 2019JZZY011104]; College Youth Innovation Science and Technology Support Program of Shandong province [grant number 2020KJK003]; Shandong Province Higher Educational Youth Innovation Talents Introduction and Cultivation Program-Chemical Biology Research Innovation Team [grant number 2019-063]; and Scientific Foundation of Binzhou Medical University [grant number BY2019KYQD47]. We would like to thank Editage for professional language editing services.

■ REFERENCES

(1) Chen, S.; Zhang, M.; Shao, X.; Wang, X.; Zhang, L.; Xu, P.; Zhong, W.; Zhang, Lu.; Xing, M.; Zhang, L. A laminin mimetic peptide SIKVAV-conjugated chitosan hydrogel promoting wound healing by enhancing angiogenesis, re-epithelialization and collagen deposition. *J. Mater. Chem. B* **2015**, *3*, 6798−6804.

(2) Naik, S.; Larsen, S. B.; Gomez, N. C.; Alaverdyan, K.; Sendoel, A.; Yuan, S.; Polak, P.; Kulukian, A.; Chai, S.; Fuchs, E. Inflammatory memory sensitizes skin epithelial stem cells to tissue damage. *Nature* **2017**, *550*, 475−480.

(3) Chen, S.; Liu, B.; Carlson, M. A.; Gombart, A. F.; Reilly, D. A.; Xie, J. Recent advances in electrospun nanofibers for wound healing. *Nanomedicine* **2017**, *12*, 1335−1352.

(4) Han, W.; Han, X.; Liu, Z.; Zhang, S.; Li, Y.; Lu, J.; Chen, J.; Ou, L.; Fu, G. Facile modification of protein-imprinted polydopamine coatings over nanoparticles with enhanced binding selectivity. *Chem. Eng. J.* **2020**, *385*, 123463.

(5) Sen, C. K.; Gordillo, G. M.; Roy, S.; Kirsner, R.; Lambert, L.; Hunt, T. K.; Gottrup, F.; Gurtner, G. C.; Longaker, M. T. Human skin wounds: a major and snowballing threat to public health and the economy. *Wound Repair Regen.* **2009**, *17*, 763−771.

(6) Coventry, C. A.; Vaska, A. I.; Holland, A. J. A.; Read, D. J.; Ivers, R. Q. Surgical procedures performed by emergency medical teams in

sudden-onset disasters: A systematic review. *World J. Surg.* **2019**, *43*, 1226−1231.
(7) Martin, P. Wound healing–aiming for perfect skin regeneration. *Science* **1997**, *276*, 75−81.
(8) Guo, B.; Dong, R.; Liang, Y.; Li, M. Haemostatic materials for wound healing applications. *Nat. Rev. Chem* **2021**, *5*, 773−791.
(9) Mascharak, S.; desJardins-Park, H. E.; Davitt, M. F.; Griffin, M.; Borrelli, M. R.; Moore, A. L.; Chen, K.; Duoto, B.; Chinta, M.; Foster, D. S.; et al. Preventing Engrailed-1 activation in fibroblasts yields wound regeneration without scarring. *Science* **2021**, *372*, No. eaba2374.
(10) Arno, A. I.; Gauglitz, G. G.; Barret, J. P.; Jeschke, M. G. Up-to-date approach to manage keloids and hypertrophic scars: a useful guide. *Burns* **2014**, *40*, 1255−1266.
(11) Liang, Y.; Li, Z.; Huang, Y.; Yu, R.; Guo, B. Dual-Dynamic-Bond Cross-Linked Antibacterial Adhesive Hydrogel Sealants with On-Demand Removability for Post-Wound-Closure and Infected Wound Healing. *ACS Nano* **2021**, *15*, 7078−7093.
(12) Hong, Y.; Zhou, F.; Hua, Y.; Zhang, X.; Ni, C.; Pan, D.; Zhang, Y. Q.; Jiang, D.; Yang, L.; Lin, Q.; et al. A strongly adhesive hemostatic hydrogel for the repair of arterial and heart bleeds. *Nat. Commun.* **2019**, *10*, 2060.
(13) Ma, Y.; Yao, J.; Liu, Q.; Han, T.; Zhao, J.; Ma, X.; Tong, Y.; Jin, G.; Qu, K.; Li, B.; Xu, F. Liquid bandage harvests robust adhesive, hemostatic, and antibacterial performances as a first-aid tissue adhesive. *Adv. Funct. Mater.* **2020**, *30*, 2001820.
(14) Wang, L.; Yang, J.; Ran, B.; Yang, X.; Zheng, W.; Long, Y.; Jiang, X. Small molecular TGF-β1-inhibitor-loaded electrospun fibrous scaffolds for preventing hypertrophic scars. *ACS Appl. Mater. Interfaces* **2017**, *9*, 32545−32553.
(15) Mojsiewicz-Pieńkowska, K.; Jamrógiewicz, M.; Żebrowska, M.; Mikolaszek, B.; Sznitowska, M. Double layer adhesive silicone dressing as a potential dermal drug delivery film in scar treatment. *Int. J. Pharm.* **2015**, *481*, 18−26.
(16) Wokovich, A. M.; Prodduturi, S.; Doub, W. H.; Hussain, A. S.; Buhse, L. F. Transdermal drug delivery system (TDDS) adhesion as a critical safety, efficacy and quality attribute. *Eur. J. Pharm. Biopharm.* **2006**, *64*, 1−8.
(17) Pikuła, M.; Żebrowska, M. E.; Pobłocka-Olech, L.; Krauze-Baranowska, M.; Sznitowska, M.; Trzonkowski, P. Effect of enoxaparin and onion extract on human skin fibroblast cell line - therapeutic implications for the treatment of keloids. *Pharm. Biol.* **2014**, *52*, 262−267.
(18) Kurian, P.; Kasibhatla, B.; Daum, J.; Burns, C.; Moosa, M.; Rosenthal, K.; Kennedy, J. Synthesis, permeability and biocompatibility of tricomponent membranes containing polyethylene glycol, polydimethylsiloxane and polypentamethylcyclopentasiloxane domains. *Biomaterials* **2003**, *24*, 3493−3503.
(19) Juárez-Moreno, J.; Ávila-Ortega, A.; Oliva, A.; Avilés, F.; Cauich-Rodríguez, J. Effect of wettability and surface roughness on the adhesion properties of collagen on PDMS films treated by capacitively coupled oxygen plasma. *Appl. Surf. Sci.* **2015**, *349*, 763−773.
(20) Agarwal, A.; Nelson, T. B.; Kierski, P. R.; Schurr, M. J.; Murphy, C. J.; Czuprynski, C. J.; McAnulty, J. F.; Abbott, N. L. Polymeric multilayers that localize the release of chlorhexidine from biologic wound dressings. *Biomaterials* **2012**, *33*, 6783−6792.
(21) Ioannou, C. J.; Hanlon, G. W.; Denyer, S. P. Action of disinfectant quaternary ammonium compounds against Staphylococcus aureus. *Antimicrob. Agents Chemother.* **2007**, *51*, 296−306.
(22) Majumdar, P.; Lee, E.; Gubbins, N.; Christianson, D. A.; Stafslien, S. J.; Daniels, J.; VanderWal, L.; Bahr, J.; Chisholm, B. J. Combinatorial materials research applied to the development of new surface coatings XIII: an investigation of polysiloxane antimicrobial coatings containing tethered quaternary ammonium salt groups. *J. Comb. Chem.* **2009**, *11*, 1115−1127.
(23) Ahlström, B.; Thompson, R. A.; Edebo, L. The effect of hydrocarbon chain length, pH, and temperature on the binding and bactericidal effect of amphiphilic betaine esters on Salmonella typhimurium. *Acta Pathol. Microbiol. Immunol. Scand.* **1999**, *107*, 318−324.
(24) Tomlinson, E.; Brown, M. R.; Davis, S. S. Effect of colloidal association on the measured activity of alkylbenzyldimethylammonium chlorides against Pseudomonas aeruginosa. *J. Med. Chem.* **1977**, *20*, 1277−1282.
(25) Pant, R. R.; Buckley, J. L.; Fulmer, P. A.; Wynne, J. H.; McCluskey, D. M.; Phillips, J. P. Hybrid siloxane epoxy coatings containing quaternary ammonium moieties. *J. Appl. Polym. Sci.* **2008**, *110*, 3080−3086.
(26) Gottenbos, B.; van der Mei, H. C.; Klatter, F.; Nieuwenhuis, P.; Busscher, H. J. In vitro and in vivo antimicrobial activity of covalently coupled quaternary ammonium silane coatings on silicone rubber. *Biomaterials* **2002**, *23*, 1417−1423.
(27) Sauvet, G.; Fortuniak, W.; Kazmierski, K.; Chojnowski, J. Amphiphilic block and statistical siloxane copolymers with antimicrobial activity. *J. Polym. Sci., Part A: Polym. Chem.* **2003**, *41*, 2939−2948.
(28) Xie, X.; Li, D.; Su, C.; Cong, W.; Mo, X.; Hou, G.; Wang, C. Functionalized biomimetic composite nanfibrous scaffolds with antibacterial and hemostatic efficacy for facilitating wound healing. *J. Biomed. Nanotechnol.* **2019**, *15*, 1267−1279.
(29) Saiding, Q.; Jin, J.; Qin, M.; Cai, Z.; Lu, M.; Wang, F.; Cui, W.; Chen, X. Heat-shrinkable electrospun fibrous tape for restoring structure and function of loose soft tissue. *Adv. Funct. Mater.* **2021**, *31*, 2007440.
(30) Chen, L.; Cheng, L.; Wang, Z.; Zhang, J.; Mao, X.; Liu, Z.; Zhang, Y.; Cui, W.; Sun, X. Conditioned medium-electrospun fiber biomaterials for skin regeneration. *Bioact. Mater.* **2021**, *6*, 361−374.
(31) Zhan, Y.; Zeng, W.; Jiang, G.; Wang, Q.; Shi, X.; Zhou, Z.; Deng, H.; Du, Y. Construction of lysozyme exfoliated rectorite-based electrospun nanofibrous membranes for bacterial inhibition. *J. Appl. Polym. Sci.* **2015**, *132*, 41496.
(32) Zhou, Y.; Yang, H.; Liu, X.; Mao, J.; Gu, S.; Xu, W. Electrospinning of carboxyethyl chitosan/poly(vinyl alcohol)/silk fibroin nanoparticles for wound dressings. *Int. J. Biol. Macromol.* **2013**, *53*, 88−92.
(33) Li, W.; Li, X.; Chen, Y.; Li, X.; Deng, H.; Wang, T.; Huang, R.; Fan, G. Poly(vinyl alcohol)/sodium alginate/layered silicate based nanofibrous mats for bacterial inhibition. *Carbohydr. Polym.* **2013**, *92*, 2232−2238.
(34) Xiao, S.; Shen, M.; Guo, R.; Huang, Q.; Wang, S.; Shi, X. Fabrication of multiwalled carbon nanotube-reinforced electrospun polymer nanofibers containing zero-valent iron nanoparticles for environmental applications. *J. Mater. Chem.* **2010**, *20*, 5700−5708.
(35) Son, W. K.; Youk, J. H.; Lee, T. S.; Park, W. H. Effect of pH on electrospinning of poly(vinyl alcohol). *Mater. Lett.* **2005**, *59*, 1571−1575.
(36) Discher, D. E.; Janmey, P.; Wang, Y. L. Tissue cells feel and respond to the stiffness of their substrate. *Science* **2005**, *310*, 1139−1143.
(37) Ma, K.; Chan, C. K.; Liao, S.; Hwang, W. Y.; Feng, Q.; Ramakrishna, S. Electrospun nanofiber scaffolds for rapid and rich capture of bone marrow-derived hematopoietic stem cells. *Biomaterials* **2008**, *29*, 2096−2103.
(38) Morris, D. E.; Wu, L.; Zhao, L. L.; Bolton, L.; Roth, S. I.; Ladin, D. A.; Mustoe, T. A. Acute and chronic animal models for excessive dermal scarring: quantitative studies. *Plast. Reconstr. Surg.* **1997**, *100*, 674−681.
(39) Weng, W.; He, S.; Song, H.; Li, X.; Cao, L.; Hu, Y.; Cui, J.; Zhou, Q.; Peng, H.; Su, J. Aligned carbon nanotubes reduce hypertrophic scar via regulating cell behavior. *ACS Nano* **2018**, *12*, 7601−7612.
(40) Cheng, L.; Wang, Y.; Sun, G.; Wen, S.; Deng, L.; Zhang, H.; Cui, W. Hydration-enhanced lubricating electrospun nanofibrous membranes prevent tissue adhesion. *Research* **2020**, *2020*, 4907185.
(41) Shah, M.; Revis, D.; Herrick, S.; Baillie, R.; Thorgeirson, S.; Ferguson, M.; Roberts, A. Role of elevated plasma transforming growth factor-beta1 levels in wound healing. *Am. J. Pathol.* **1999**, *154*, 1115−1124.

https://doi.org/10.1021/acsomega.2c03222
ACS Omega 2022, 7, 30137−30148

(42) Shah, M.; Foreman, D. M.; Ferguson, M. W. Neutralising antibody to TGF-beta 1,2 reduces cutaneous scarring in adult rodents. *J. Cell Sci.* **1994**, *107*, 1137−1157.
(43) Berman, B.; Maderal, A.; Raphael, B. Keloids and hypertrophic scars: Pathophysiology, classification, and treatment. *Dermatol. Surg.* **2017**, *43*, S3−S18.
(44) Friedman, D. W.; Boyd, C. D.; Mackenzie, J. W.; Norton, P.; Olson, R. M.; Deak, S. B. Regulation of collagen gene expression in keloids and hypertrophic scars. *J. Surg. Res.* **1993**, *55*, 214−222.
(45) Naitoh, M.; Hosokawa, N.; Kubota, H.; Tanaka, T.; Shirane, H.; Sawada, M.; Nishimura, Y.; Nagata, K. Upregulation of HSP47 and collagen type III in the dermal fibrotic disease, keloid. *Biochem. Biophys. Res. Commun.* **2001**, *280*, 1316−1322.

https://doi.org/10.1021/acsomega.2c03222
ACS Omega 2022, 7, 30137−30148